

Depth-aware Fusion Method based on Image and 4D Radar Spectrum for 3D Object Detection

Yue Sun¹, Yeqiang Qian^{*2,3}, Chunxiang Wang^{2,3} and Ming Yang^{2,3}

Abstract—Safety and reliability are crucial for the public acceptance of autonomous driving. To ensure accurate and reliable environmental perception, intelligent vehicles must exhibit accuracy and robustness in various environments. Millimeter-wave radar, known for its high penetration capability, can operate effectively in adverse weather conditions such as rain, snow, and fog. Traditional 3D millimeter-wave radars can only provide range, Doppler, and azimuth information for objects. Although the recent emergence of 4D millimeter-wave radars has added elevation resolution, the radar point clouds remain sparse due to Constant False Alarm Rate (CFAR) operations. In contrast, cameras offer rich semantic details but are sensitive to lighting and weather conditions. Hence, this paper leverages these two highly complementary and cost-effective sensors, 4D millimeter-wave radar and camera. By integrating 4D radar spectra with depth-aware camera images and employing attention mechanisms, we fuse texture-rich images with depth-rich radar data in the Bird’s Eye View (BEV) perspective, enhancing 3D object detection. Additionally, we propose using GAN-based networks to generate depth images from radar spectra in the absence of depth sensors, further improving detection accuracy.

I. INTRODUCTION

Safety and reliability are key factors for the widespread acceptance of autonomous driving technology. Hence, developing robust all-weather environmental perception algorithms is essential. Common sensors used in autonomous driving for 3D object detection include cameras, LiDAR, and millimeter-wave radar. Cameras can provide rich visual information such as color and texture but are sensitive to lighting and weather. LiDAR offers dense point clouds but faces limitations in adverse weather and is high-cost. Millimeter-wave radar performs exceptionally well under challenging conditions, is cost-effective, and can measure speed and detect objects at long ranges, making it promising for autonomous driving [1]. However, its main challenge is the sparsity of measurements, exacerbated by traditional processing methods like Side Lobe Suppression (SLS) [2] and Constant False Alarm Rate (CFAR) [3], leading to severe information loss. Recent advancements in 4D millimeter-wave radar provide elevation information but still suffer from low data density and noise.

To achieve accurate and reliable perception, autonomous vehicles typically fuse data from multiple sensor modalities for environmental perception and 3D object detection.

† This work is supported by the National Natural Science Foundation of China (62103261/62173228/62373250).

¹ The Global Institute of Future Technology, Shanghai Jiao Tong University, Shanghai, 200240, China.

² The Department of Automation, Shanghai Jiao Tong University, Shanghai, 200240, China.

³ Key Laboratory of System Control and Information Processing, Ministry of Education of China, Shanghai, 200240, China.

* Corresponding author: Yeqiang Qian
qianyeqiang@sjtu.edu.cn.

Fusing signals from cameras and millimeter-wave radars enables achieving a comprehensive and cost-effective perception of the surrounding environment in terms of contours, color, texture, distance, and speed. Additionally, the fusion system can operate continuously under all weather conditions and varying light levels. However, challenges remain in fusing camera and radar signals [4]. Millimeter-wave radar data can be represented in various data formats depending on the processing stage, including raw ADC signals, radar spectra after applying Fast Fourier Transform (FFT) on ADC signals, and radar point clouds after further applying SLS and CFAR operations [5]. Currently, radar point clouds are mostly used in 3D object detection algorithms but face issues due to their high sparsity and inherent differences from LiDAR point clouds, making them less effective for detection tasks. Moreover, there are challenges related to camera-radar sensor fusion in terms of resolution variations and perceived dimensionality [4].

To address the aforementioned issues, this paper proposes using raw 4D radar spectra and depth-aware images as input data. Features are extracted separately from the RGB and depth images to obtain corresponding multi-scale features, which are then fused to produce multi-scale image features with depth information. Following a similar approach to EchoFusion [6], image and radar features are fused in the BEV feature space under polar coordinates based on column-wise attention for image features and row-wise cross-attention for radar features, aggregating high resolution of image features in the elevation direction and radar features in the depth direction. The resulting BEV features and object queries are then applied in the polar decoder [7] and detection head for 3D object predictions.

The main contributions of this paper are as follows:

- 1) We propose an all-weather object detection algorithm that integrates depth-aware images and 4D millimeter-wave radar spectra in the BEV feature space to achieve optimal 3D object detection performance.
- 2) We introduce a method to augment features from RGB images with depth images before camera-radar data fusion, and we propose using a GAN-based depth generator to produce depth images from radar spectra when a depth sensor is unavailable.
- 3) Our model achieves good detection performance while significantly reducing network complexity.

II. RELATED WORK

A. Radar Data Representations

Millimeter-wave radar uses radio waves in the millimeter-wave frequency range (30 GHz to 300 GHz)

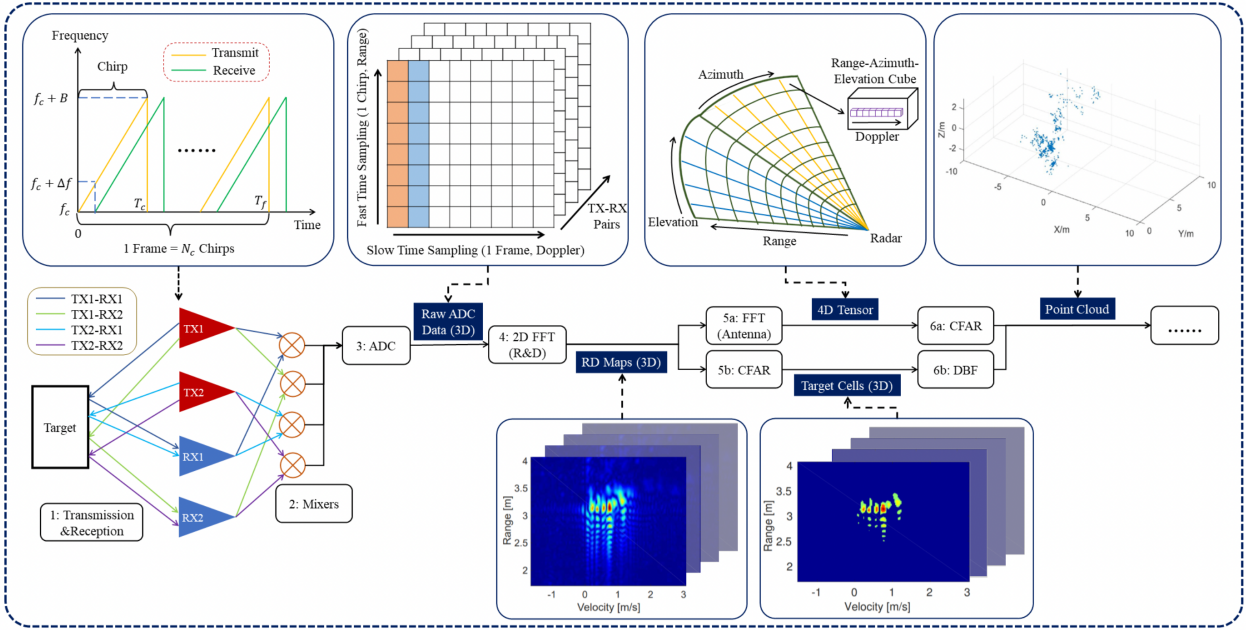


Fig. 1. Traditional signal processing pipeline of 4D millimeter-wave radar data and the corresponding data format after each step [1].

for environmental sensing. Typically, each transmitting antenna (TX) emits a sequence of Frequency Modulated Continuous Waves (FMCW), called chirps, with linearly increasing frequency [8]. Reflected waves from objects are captured by receiving antennas (RX) and processed to determine distance, speed, and angle. Traditional 3D radars, with horizontally arranged antennas, provide only horizontal detection and lack elevation information. In contrast, 4D radars use both horizontal and vertical antenna arrays, enabling the measurement of elevation angles as well. 4D radar data can be represented as ADC signals, radar spectra, or point clouds, depending on the processing stage.

Fig. 1 shows the traditional process of converting 4D millimeter-wave radar signals from raw reflected waves to radar point clouds, along with the corresponding data format at each step.

- Step 1: Each radar TX sends chirps, and each RX receives the reflected signals.
- Step 2: The received signal and its corresponding transmitted signal are mixed and passed through a low-pass filter to generate an Intermediate Frequency (IF) signal.
- Step 3: The IF signal is converted into raw ADC data by an Analog-to-Digital Converter.
- Step 4: Apply FFT to the ADC data along the range and Doppler dimensions to produce a series of Range-Doppler (RD) maps corresponding to different TX-RX pairs.
- Step 5 & 6: One approach is to apply FFT along the azimuth and elevation dimensions of different TX-RX pairs to obtain a 4D radar spectrum (Step 5a). Then, in Step 6a, CFAR operation is applied to the four-dimensional data to filter it based on intensity, resulting in a radar point cloud. Another approach is to first apply a CFAR-type algorithm to filter the RD map and generate target cells (Step 5b), and then

use Digital Beamforming (DBF) in Step 6b to recover angle information and generate the radar point cloud.

B. Camera-Radar Datasets

Although many public datasets now include millimeter-wave radar data alongside images and LiDAR data, these radar datasets contain fewer samples compared to the latter two. Most existing datasets, such as NuScenes [9], RADDet [10], Zendar [11], RADIATE [12], and CAR-RADA [13], use traditional 3D radar, providing data along the range, Doppler, and azimuth dimensions but lacking elevation information. This limitation makes accurate 3D bounding box estimation challenging in 3D object detection. With the emergence of 4D millimeter-wave radar, more public datasets have begun incorporating 4D radar to capture data with elevation information.

However, most of these datasets provide radar point clouds processed by methods like CFAR, such as View-of-Delft [14], Astyx [15], and RadarScenes [16]. Due to the sparsity of radar signals, we aim to use 4D radar that provides elevation information, and the radar data should be in the form of lossless *raw radar data* before CFAR operations, including ADC data and radar spectra. Among available datasets, RADIal and K-Radar meet these criteria. However, RADIal initially only offered 2D annotations, and although Liu et al. [6] recently added 3D annotations, it remains limited in scope and lacks data under adverse weather conditions. Therefore, the K-Radar dataset is the most suitable for this research.

K-Radar contains 35K frames of 4D radar spectrum/tensor (4DRT) with measurements across the range, Doppler, azimuth, and elevation dimensions, alongside multi-view images, high-resolution LiDAR point clouds, annotated 3D bounding boxes, and other relevant data. K-Radar also covers various challenging road structures (e.g., urban, suburban roads, alleyways, and highways) and adverse weather conditions (e.g., fog, rain, and snow) [17].

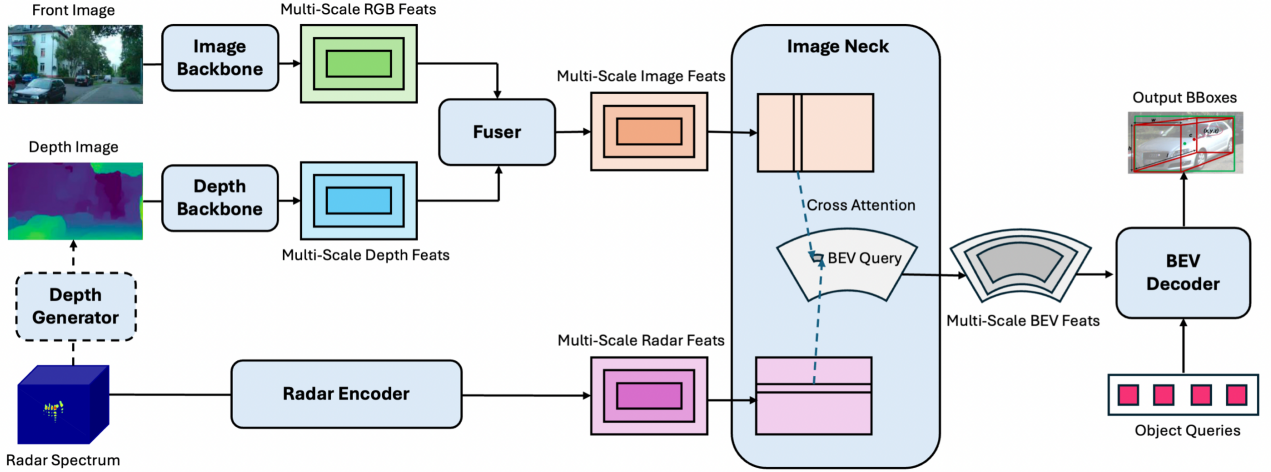


Fig. 2. The overall architecture of our proposed algorithm.

C. Camera-Radar Fusion based 3D Object Detection

Previous radar-camera fusion-based 3D object detection algorithms often rely on traditional 3D millimeter-wave radar signals, which are typically represented as radar point clouds. Methods like CenterFusion [18], RCBEVDet [19], and BEVFusion [20] extract radar features similar to LiDAR and then fuse them with image features through concatenation or cross-attention before feeding them into the detection network. However, these traditional 3D radar point clouds lack elevation information and lose significant data due to CFAR thresholding, which negatively impacts the model’s detection performance. As a result, researchers often prefer high-resolution sensors like cameras and LiDARs for multisensor fusion to achieve better detection performance.

With the emergence of 4D millimeter-wave radars, many studies have begun fusing more cost-effective and highly complementary cameras and 4D millimeter-wave radars in 3D object detection algorithms. Methods such as LXL [21] and RCFusion [22] fuse 4D radar point clouds with image features by first pillarizing the radar point clouds to extract BEV features, which are then fused with image features in the BEV feature space. To mitigate the information loss inherent in radar point clouds, EchoFusion [6] and DPFT [4] propose fusing raw radar data with camera images. However, EchoFusion has high computational resource demands (requiring 4.0 GiB of GPU memory during the inference stage [4]), while DPFT uses a full 4D tensor as input, which requires significant memory, and is difficult to obtain [17]. Building on EchoFusion’s work, our method enhances image features with depth information before radar-camera fusion, which can improve 3D object detection performance while reducing network complexity. Additionally, we propose that depth information can still be derived from 4D radar spectra even in the absence of a depth sensor.

III. METHODOLOGY

A. System Overview

Our overall architecture is illustrated in Fig. 2. It takes depth-aware images from a front camera and radar spectra from a 4D millimeter-wave radar as inputs. For the radar

spectrum input branch, we use a convolutional neural network (CNN) to extract multi-scale radar features. For the image input branch, we first separately extract multi-scale features from RGB images and depth images, and then fuse these features to obtain multi-scale image features with depth information. In the BEV space under polar coordinates, polar queries at each scale fuse image features and radar features at that scale through an attention mechanism to produce multi-scale BEV features. Finally, the multi-scale BEV features and object queries are fed into the polar decoder [7] and detection heads to estimate the classes and bounding boxes of 3D objects.

B. RGB and Depth Images Fusion

Since each pixel value in a depth image represents the spatial depth information of the corresponding location of the object, while each pixel value in an RGB image corresponds to the color and texture information, feature extraction should be performed separately for each. We preprocess the single-channel depth image by expanding it to three channels through simple repetition. Then, we use the lightweight convolutional network ResNet18 [23] as the backbone to extract multi-scale features from both RGB and depth images. The resulting multi-scale features are concatenated along the channel dimension and fed into a Feature Pyramid Network (FPN) [24] for feature fusion, which outputs multi-scale image features with depth information.

C. Image and Radar Feature Fusion

For the BEV feature space at the l -level in the polar coordinate system, we first initialize it uniformly with $R^l \times A^l$ BEV queries, where R^l and A^l are the range and azimuth resolutions of the BEV features at level l , and each query is represented as $q^l(r_{bev}, \phi_{bev})$.

The fusion of image feature F_I^l and radar feature F_R^l is based on the fact that each polar column with the same azimuth ϕ_{bev} in the BEV features corresponds to a column x_i^l in the image feature, and each polar row with the same range r_{bev} in the BEV features corresponds to a row in the radar feature R_r^l . Following the polar-aligned Attention (PAA) technique proposed in EchoFusion [6], we fuse the image and radar features as follows:

We use cross-attention to update the BEV queries with image features as follows:

$$\hat{Q}^l = \text{CrossAttention}(Q_1^l, K_1^l, V_1^l) \quad (1)$$

$$Q_1^l = \text{all } q^l(r_{bev}, \phi_{bev}) \text{ with the same } \phi_{bev} \quad (2)$$

$$K_1^l = V_1^l = \text{all } f_I^l(x_I, y_I) \text{ with the same } x_I \quad (3)$$

Then, we update the BEV queries with radar features based on:

$$\tilde{Q}^l = \text{CrossAttention}(Q_2^l, K_2^l, V_2^l) \quad (4)$$

$$Q_2^l = \text{all } \hat{q}^l(r_{bev}, \phi_{bev}) \text{ with the same } r_{bev} \quad (5)$$

$$K_2^l = V_2^l = \text{all } f_R^l(a_I, r_I) \text{ with the same } r_I \quad (6)$$

D. Depth Image Generation From Radar Spectrum

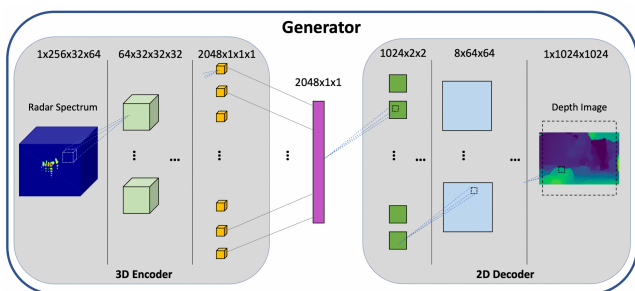


Fig. 3. The network architecture of our depth image generator based on the design proposed in [25].

Depth images are vital for improving the accuracy of vision-based object detection [26]. While depth sensors usually provide these images, they are sometimes absent in autonomous vehicles due to size and cost constraints. Inspired by work in [25], [27], [28], we propose using a GAN-based depth generator to generate accurate depth images with high resolution from millimeter-wave radar spectra. By generating depth images before applying attention-based feature fusion, we can augment images with depth information, allowing image features to include depth information and thereby improve our model’s overall detection performance. The depth generator network is similar to the one in [25], except that skip connections are not used in the generator (as shown in Fig. 3). The training data comes from K-Radar sequences 12-20, with ground truth depth obtained by projecting LiDAR point clouds onto images.

E. Detection Head and Loss

We use a similar architecture as used in [6] and [7], but with the number of decoder layers reduced from 6 to 3, and we limit the object queries to 20 instead of 30 to minimize computation consumption. The resulting object queries are then fed into classification and regression detection heads to obtain the predicted categories c and 3D bounding boxes $\vec{b} = (x, y, z, l, w, h, \phi)$ of detected 3D objects.

During model training, a Hungarian matching-based set-to-set loss is employed, which consists of Focal Loss for the classification network and L1 Loss for the regression network.

IV. EXPERIMENTS

A. Dataset

We use a subset of the K-Radar dataset [17], specifically sequences 1-11, for our experiments. This choice is due to the fact that only sequences 1-20 have been uploaded to Google Drive and are readily accessible. Additionally, we initially reserved sequences 12-20 for training the depth generator.

B. Model Training and Testing

We conduct all experiments on two NVIDIA GeForce RTX 3090 GPUs with a batch size of 4. Due to the limited size of our dataset, we reorganize the training and testing sets. A total of 7,755 frames from K-Radar sequences 1-11 are split into an approximately 9:1 ratio, with 6,972 frames used for training and 783 frames for testing. We follow the same training strategy as used in [6], but we train the model for only 10 epochs as we use about half the data they used for training. Given the limited hardware resources and the relatively large network structure, we restrict our training and testing to the *Sedan* category, which predominates in K-Radar sequences 1-11, accounting for over 77.3% of all objects.

C. Evaluation Results

We evaluate the following models on our test dataset as mentioned in Subsection IV-B.

- *EchoFusion* [6]: Configured with its default settings.
- *EchoFusion-small*: A *light* version of EchoFusion, featuring a *smaller* network as used in our model that replaces ResNet50 with ResNet18, reduces the number of decoder layers from 6 to 3, and utilizes only 20 object queries instead of 30.
- *Ours-depth64*: Our model, as described in Section III, with the input depth images generated by projecting 64-line LiDAR point clouds onto the images.
- *Ours-depth128*: The same as *Ours-depth64*, but using 128-line LiDAR instead.

TABLE I
EVALUATION OF DETECTION PERFORMANCE USING DIFFERENT METHODS.

Method	BEV AP (%)			3D AP(%)		
	0.3	0.5	0.7	0.3	0.5	0.7
EchoFusion	90.82	90.73	89.78	90.79	88.26	58.70
EchoFusion-small	90.43	90.19	78.95	90.36	79.08	47.73
Ours-depth64	98.99	89.97	88.38	90.60	88.51	70.58
Ours-depth128	99.75	90.65	88.97	99.63	89.06	61.44

We use the KITTI protocol to evaluate the Average Precision (AP) of all the models mentioned above, with Intersection over Union (IoU) thresholds set at 0.3, 0.5, and 0.7. We highlight the best result for each metric in bold. As shown in Table I, Ours-depth128 and Ours-depth64 significantly outperform EchoFusion-small in all AP metrics except for the BEV AP at a threshold of 0.5. Moreover, while our methods are slightly inferior to EchoFusion in the BEV AP at thresholds of 0.5 and 0.7, both Ours-depth128 and Ours-depth64 surpass EchoFusion in all the

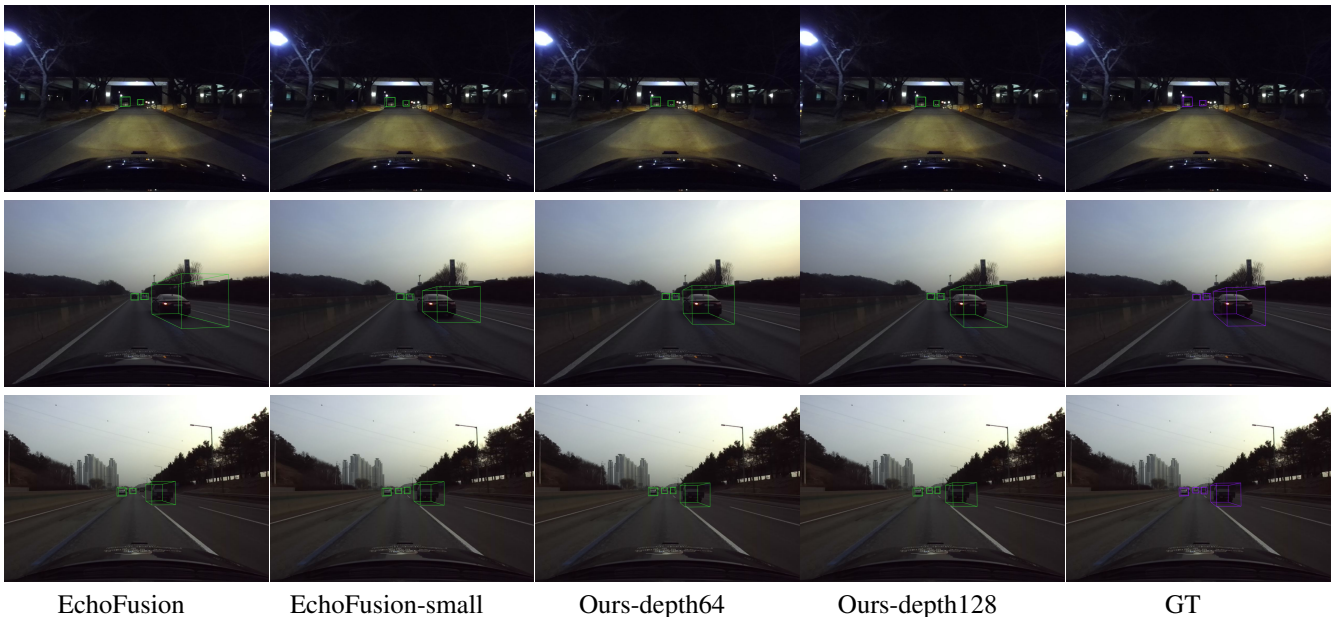


Fig. 4. Visualization of outputs from different methods compared to ground truth.

3D AP metrics, except when the 3D AP threshold is 0.3, where Ours-depth64 is slightly inferior to EchoFusion. When the threshold is set at 0.3, both the BEV AP and 3D AP of Ours-depth128 exceed EchoFusion by more than 10%.

We present the errors for the outputs of all models in Table II. Using an evaluation method similar to that of NuScenes, we first match the output bounding boxes with the ground truth. We then calculate the average Euclidean distance between the centers of the output and ground truth (GT) bounding boxes as the Average Translation Error (ATE), the average ratio of their diagonal lengths as the Average Scaling Error (ASE), and the average difference in their angles as the Average Orientation Error (AOE). The table indicates that, except for the slightly larger angle error in Ours-depth128, all the error metrics of our methods are lower than those of EchoFusion and EchoFusion-small.

TABLE II
PREDICTION ERRORS USING DIFFERENT METHODS.

Method	ATE (meter)	ASE (%)	AOE (degree)
EchoFusion	0.25	6.30	7.74
EchoFusion-small	0.29	8.08	7.92
Ours-depth64	0.23	6.27	7.34
Ours-depth128	0.23	6.23	7.99

We also visualize the projected bounding boxes of each model’s output alongside the ground truth in the images, as shown in Fig. 4. This indicates that, in most cases, all models produce similar predictions, but there are some subtle differences in certain scenarios. For instance, in the second row, the bounding boxes predicted by our methods appear more accurate in terms of size and angle. In the third row, EchoFusion fails to detect a distant object, whereas this issue is not observed with the other methods.

The results above demonstrate that our models significantly improve detection performance by incorporating depth images to enhance image features. It is also worth

noting that our models are smaller compared to EchoFusion: our models use approximately 19 GiB of memory during training on an RTX 3090, while EchoFusion requires about 24 GiB. During inference, our models utilize 3.8 GiB, whereas EchoFusion uses 4.1 GiB.

D. Discussion and Limitation

As mentioned in Subsection III-D, inspired by 3DRIMR [25], in the absence of a depth sensor, we can generate corresponding depth images from radar spectra using a GAN-based depth generator. If we disregard network complexity, we could directly integrate the depth generator into the existing model, as shown in Fig. 2. Alternatively, to avoid adding extra parameters, we could first train the depth generator on a subset of the data and then load the pre-trained depth generator into the existing model to generate the depth images. This approach is feasible, as the depth images generated in 3DRIMR [25] are of high quality. However, since the K-Radar dataset lacks depth images, we can only project point clouds from a 64-line and a 128-line LiDAR onto the images to create ground truth depth images. These depth images are very sparse, and combined with the limited data available (approximately 4,500 frames for training in our experiments), the current depth generator we have trained cannot output high-quality depth images. We aim to address this issue in the future.

V. CONCLUSION AND FUTURE WORK

In this work, we propose a novel 3D object detection algorithm based on the fusion of cameras and 4D millimeter-wave radar for multimodal perception. This approach aims to enhance detection performance, cost-effectiveness, and robustness in all-weather environments. We are the first to utilize depth-aware images and 4D millimeter-wave radar spectra as inputs for 3D object detection, and we propose generating depth images from radar spectra when depth sensors are unavailable. Experimental results demonstrate that our model maintains strong detection performance while requiring less memory and computational resources.

However, while numerous studies have shown that using raw radar data can yield better detection performance compared to radar point clouds, raw radar data also requires significant storage capacity and contains considerable noise. In the future, we aim to explore radar data preprocessing techniques to reduce the size of the radar spectrum and remove noise before inputting it into the model.

REFERENCES

- [1] L. Fan, J. Wang, Y. Chang, Y. Li, Y. Wang, and D. Cao, "4d mmwave radar for autonomous driving perception: A comprehensive survey," *IEEE Transactions on Intelligent Vehicles*, vol. 9, no. 4, pp. 4606–4620, 2024.
- [2] H. Yang and J. Wang, "Sidelobe suppression of sar images by spectrum shaping," pp. 1668–1671, 2022.
- [3] H. Rohling, "Radar cfar thresholding in clutter and multiple target situations," *IEEE Transactions on Aerospace and Electronic Systems*, vol. AES-19, no. 4, pp. 608–621, 1983.
- [4] F. Fent, A. Palffy, and H. Caesar, "Dpft: Dual perspective fusion transformer for camera-radar-based object detection," *arXiv preprint arXiv:2404.03015*, 2024.
- [5] S. Yao, R. Guan, Z. Peng, C. Xu, Y. Shi, W. Ding, E. G. Lim, Y. Yue, H. Seo, K. L. Man, J. Ma, X. Zhu, and Y. Yue, "Exploring radar data representations in autonomous driving: A comprehensive review," 2024. [Online]. Available: <https://arxiv.org/abs/2312.04861>
- [6] Y. Liu, F. Wang, N. Wang, and Z. Zhang, "Echoes beyond points: Unleashing the power of raw radar data in multi-modality fusion," 2023.
- [7] Y. Jiang, L. Zhang, Z. Miao, X. Zhu, J. Gao, W. Hu, and Y.-G. Jiang, "Polarformer: multi-camera 3d object detection with polar transformer," in *AAAI*, ser. AAAI'23/IAAI'23/EAAI'23. AAAI Press, 2023.
- [8] C. Iovescu and S. Rao, "The fundamentals of millimeter wave radar sensors," pp. 1–9, 2021.
- [9] H. Caesar, V. Bankiti, A. H. Lang, S. Vora, V. Liong, Q. Xu, A. Krishnan, Y. Pan, G. Baldan, and O. Beijbom, "nusenes: A multimodal dataset for autonomous driving," pp. 11 618–11 628, 2020.
- [10] A. Zhang, F. E. Nowruzi, and R. Laganieri, "Raddet: Range-azimuth-doppler based radar object detection for dynamic road users," pp. 95–102, 2021.
- [11] M. Mostajabi, C. M. Wang, D. Ranjan, and G. Hsyu, "High resolution radar dataset for semi-supervised learning of dynamic objects," pp. 450–457, 2020.
- [12] M. Sheeny, E. De Pellegrin, S. Mukherjee, A. Ahrabian, S. Wang, and A. Wallace, "Radiate: A radar dataset for automotive perception in bad weather." IEEE Press, 2021, p. 1–7.
- [13] A. Ouaknine, A. Newson, J. Rebut, F. Tupin, and P. Perez, "Carrada dataset: Camera and automotive radar with range- angle- doppler annotations," Los Alamitos, CA, USA, pp. 5068–5075, 2021.
- [14] A. Palffy, E. Pool, S. Baratam, J. F. P. Kooij, and D. M. Gavrilu, "Multi-class road user detection with 3+1d radar in the view-of-delft dataset," *IEEE Robotics and Automation Letters*, vol. 7, no. 2, pp. 4961–4968, 2022.
- [15] M. Meyer and G. Kuschik, "Automotive radar dataset for deep learning based 3d object detection," pp. 129–132, 2019.
- [16] O. Schumann, M. Hahn, N. Scheiner, F. Weishaupt, J. F. Tilly, J. Dickmann, and C. Wöhler, "Radarscenes: A real-world radar point cloud data set for automotive applications," pp. 1–8, 2021.
- [17] D.-H. Paek, S.-H. Kong, and K. T. Wijaya, "K-radar: 4d radar object detection for autonomous driving in various weather conditions," *Advances in Neural Information Processing Systems*, vol. 35, pp. 3819–3829, 2022.
- [18] R. Nabati and H. Qi, "Centerfusion: Center-based radar and camera fusion for 3d object detection," pp. 1526–1535, 2021.
- [19] Z. Lin, Z. Liu, Z. Xia, X. Wang, Y. Wang, S. Qi, Y. Dong, N. Dong, L. Zhang, and C. Zhu, "Rcbevdet: Radar-camera fusion in bird's eye view for 3d object detection," pp. 14 928–14 937, June 2024.
- [20] Z. Liu, H. Tang, A. Amini, X. Yang, H. Mao, D. L. Rus, and S. Han, "Befusion: Multi-task multi-sensor fusion with unified bird's-eye view representation," pp. 2774–2781, 2023.
- [21] W. Xiong, J. Liu, T. Huang, Q.-L. Han, Y. Xia, and B. Zhu, "Lxl: Lidar excluded lean 3d object detection with 4d imaging radar and camera fusion," *IEEE Transactions on Intelligent Vehicles*, vol. 9, no. 1, p. 79–92, 2024.
- [22] L. Zheng, S. Li, B. Tan, L. Yang, S. Chen, L. Huang, J. Bai, X. Zhu, and Z. Ma, "Rcfusion: Fusing 4-d radar and camera with bird's-eye view features for 3-d object detection," *IEEE Transactions on Instrumentation and Measurement*, vol. 72, pp. 1–14, 2023.
- [23] K. He, X. Zhang, S. Ren, and J. Sun, "Deep residual learning for image recognition," pp. 770–778, 2016.
- [24] T.-Y. Lin, P. Dollár, R. Girshick, K. He, B. Hariharan, and S. Belongie, "Feature pyramid networks for object detection," pp. 936–944, 2017.
- [25] Y. Sun, Z. Huang, H. Zhang, Z. Cao, and D. Xu, "3drimr: 3d reconstruction and imaging via mmwave radar based on deep learning," pp. 1–8, 2021.
- [26] A. Lopes, R. Souza, and H. Pedrini, "A survey on rgb-d datasets," *Computer Vision and Image Understanding*, vol. 222, p. 103489, 2022.
- [27] Y. Sun, H. Zhang, Z. Huang, and B. Liu, "R2p: A deep learning model from mmwave radar to point cloud," p. 329–341, 2022.
- [28] Y. Sun, Z. Huang, H. Zhang, and X. Liang, "3d reconstruction of multiple objects by mmwave radar on uav," pp. 491–495, 2022.